Journal of Materials Chemistry A

ROYAL SOCIETY OF CHEMISTRY

PAPER

View Article Online
View Journal | View Issue

Cite this: J. Mater. Chem. A, 2020, 8, 5194

Achieving organic solar cells with efficiency over 14% based on a non-fullerene acceptor incorporating a cyclopentathiophene unit fused backbone†

Yao Cai,‡[a] Lingxian Meng,‡[a] Huanhuan Gao,[a] Ziqi Guo,[a] Nan Zheng,[b] Zengqi Xie,[b] Hongtao Zhang,[a] Chenxi Li,[a] Xiangjian Wan *[a] and Yongsheng Chen[a]

Received 16th January 2020
Accepted 12th February 2020

DOI: 10.1039/d0ta00677g

rsc.li/materials-a

The cyclopentadithiophene (CPT) unit is a classic building block for constructing organic semiconductor materials with excellent performances. In this work, we designed and synthesized a new acceptor **BCPT-4F**, incorporating a CPT fused central backbone. **BCPT-4F** shows a redshift absorption in the near-infrared region compared with CPT based acceptors with an unfused backbone. Importantly, the photovoltaic device based on **PBDB-T**:**BCPT-4F** achieved a promising power conversion efficiency (PCE) of 12.43% with a high short circuit current density (J_{sc}) of 22.96 mA cm^{-2}. Furthermore, based on the above binary device, a ternary device with **F-Br** as the third component achieved a high PCE of 14.23%, which is presently the highest efficiency for devices with CPT based photovoltaic materials.

1. Introduction

In the past decade, much enthusiasm has been focused on organic photovoltaics (OPVs) due to their outstanding characteristics such as flexibility, low cost, low weight, *etc.*[1–4] Presently, the power conversion efficiencies (PCEs) of OPV cells have reached over 16% for single junction devices and over 17% for tandem cells.[5–15] This impressive progress can be mainly attributed to the rational molecular design and device optimization. In particular, the intensive study on non-fullerene acceptors (NFAs) in recent years has directly pushed forward the progress of OPVs since NFAs have advantages of easy control of absorption and energy levels in contrast with the classic fullerene acceptors. Among various types of NFAs, molecules with an acceptor–donor–acceptor (A–D–A) architecture and fused molecular backbones have been widely studied and demonstrated big success.[16–20] To date, many fused backbones composed of different building blocks have been designed for the A–D–A NFA design from the perspective of absorption, energy levels, packing mode, *etc.*[21–23]

The cyclopentadithiophene (CPT) unit is a classic unit for constructing organic semiconductors such as donor polymers due to its unique electronic properties and chemical structure.[24–26] Firstly, it is an excellent electron rich unit with strong electron donating ability. Secondly, the side-chains attached on its sp^3-carbon atoms could provide effective hindrance to prevent molecular excessive self-aggregation.[27,28] With this, CPT based acceptors have also been designed and showed promising efficiencies. For example, Chen *et al.* reported a series of CPT based acceptors with unfused structures, in which a DFPCIC based device achieved a promising PCE of 10.14% with a J_{sc} of 15.66 mA cm^{-2}.[29] Recently, Bo and coworkers have designed and synthesized an acceptor, DOC2C6-2F, incorporating a CPT unit, which showed a similar unfused backbone compared with DFPCIC and exhibited an absorption covering 600–900 nm.[30] When blended with **PBDB-T**, the DOC2C6-2F based device achieved a PCE of 13.24% with a J_{sc} of 21.35 mA cm^{-2}. Other CPT based acceptors have also been reported with promising device performance around 10%.[31] With the absorption edge below 900 nm, those unfused-ring core based acceptors incorporating CPT showed relatively lower J_{sc}, which limited further improvement of PCEs. On the other hand, it has been demonstrated that A–D–A molecules with a fused electron-donating core and strong electron acceptor end groups show strong intramolecular charge transfer (ICT) effects, which could lead to red-shifted absorptions and help to improve the J_{sc} of OPV devices.[32] However, the fused backbone strategy has rarely been employed for the design of small molecule acceptors fused with a CPT unit.[30,31,33,34]

[a]The Centre of Nanoscale Science and Technology, Key Laboratory of Functional Polymer Materials, Institute of Polymer Chemistry, State Key Laboratory of Elemento-Organic Chemistry, College of Chemistry, Renewable Energy Conversion and Storage Center (RECAST), Nankai University, Tianjin 300071, China. E-mail: xjwan@nankai.edu.cn

[b]Institute of Polymer Optoelectronic Materials and Devices, State Key Laboratory of Luminescent Materials and Devices, South China University of Technology, Guangzhou 510640, China

† Electronic supplementary information (ESI) available. See DOI: 10.1039/d0ta00677g

‡ These authors contributed equally to this work.

Based on the above analysis, herein, we have designed and synthesized an A–D–A acceptor, **BCPT-4F**, with a molecular backbone fused with two CPT units with a phenyl core (Fig. 1a and b). The fluorinated 3-(dicyanomethylidene)-indan-1-one was used as the electron-withdrawing end group. **BCPT-4F** has a low optical band gap of 1.32 eV with a near-infrared region (NIR) film absorption from 600 to 1000 nm. Compared with its analogous CPT base unfused molecules counterparts, **BCPT-4F** has an extended conjugated length and red shifted absorption.[29,30,34] When blended with the wide band gap polymer donor **PBDB-T**, the **BCPT-4F** based device exhibited a PCE of 12.43% with a J_{sc} of 22.96 mA cm^{-2}, a V_{oc} of 0.776 V and an FF of 0.698. Based on the above binary device, a ternary device was fabricated employing a middle band gap acceptor **F-Br** we reported previously.[35] After device optimization, a high PCE of 14.23% with the simultaneously increased J_{sc} of 24.88 mA cm^{-2}, V_{oc} of 0.806 V, and FF of 0.709 was obtained, which is the highest efficiency to date for devices with CPT based photovoltaic materials (Fig. 2a and Table S3†).

2. Results and discussion

2.1 Synthesis and characterization

The synthetic route for **BCPT-4F** is shown in Scheme 1. Starting from 4*H*-cyclopenta[1,2-*b*:5,4-*b*′]dithiophene **1**, we synthesized 2-(4,4-dimethyl-4*H*-cyclopenta[1,2-*b*:5,4-*b*′]dithiophen-2-yl)-4,4,5,5-tetramethyl-1,3,2-dioxaborolane **3**. Note, two methyl groups are used as side chains on the CPT sp^3 carbon in order to alleviate the hindrance in the following fused ring reaction from **4** to **5** since it could not succeed if general octyl chains were used in our lab. Finally, the targeted product **BCPT-4F** was obtained by Knoevenagel condensation between **6** and 2F-IC. **BCPT-4F** exhibited good solubility in common solvents like chloroform and chlorobenzene. The detailed synthesis steps and characterization methods including ^{1}H NMR spectroscopy, ^{13}C NMR spectroscopy and mass spectrometry are showed in the ESI.† The thermal properties of **BCPT-4F** were measured by thermogravimetric analysis (ESI, Fig. S11†) under a nitrogen atmosphere. This indicates that **BCPT-4F** exhibits good thermal stability with a weight loss lower than 5% up to 364 °C.

The solid neat film absorption spectrum for **BCPT-4F** is presented in Fig. 1c. Because of the enhanced ICT effect, **BCPT-4F** demonstrated strong absorption in the wavelength range from 600 to 1000 nm. It red-shifted by 57 nm in contrast to its solution absorption spectrum (Fig. S12†), suggesting that effective intermolecular interactions occurred in the solid film. Compared with unfused CPT based acceptors, **BCPT-4F** exhibited manifest redshifted absorption with a peak at 860 nm in the film (Table 1).[29,33,36] From the film absorption onset (~940 nm), the optical band gap of **BCPT-4F** was calculated to be 1.32 eV. Cyclic voltammetry (CV) measurements were performed to check the energy levels of the acceptor. As calculated from the onset of oxidative and reductive peaks in CV curves (Fig. S13†), the highest occupied molecular orbital (HOMO) and lowest unoccupied molecular orbital (LUMO) energy levels of **BCPT-4F** were determined to be −5.36 and −3.91 eV, respectively.

2.2 Device structure and photovoltaic properties

The OSC devices with an inverted structure of indium tin oxide (ITO)/ZnO/PFN-Br/**PBDB-T**:NFA/MoO$_x$/Ag (Fig. 2b) were

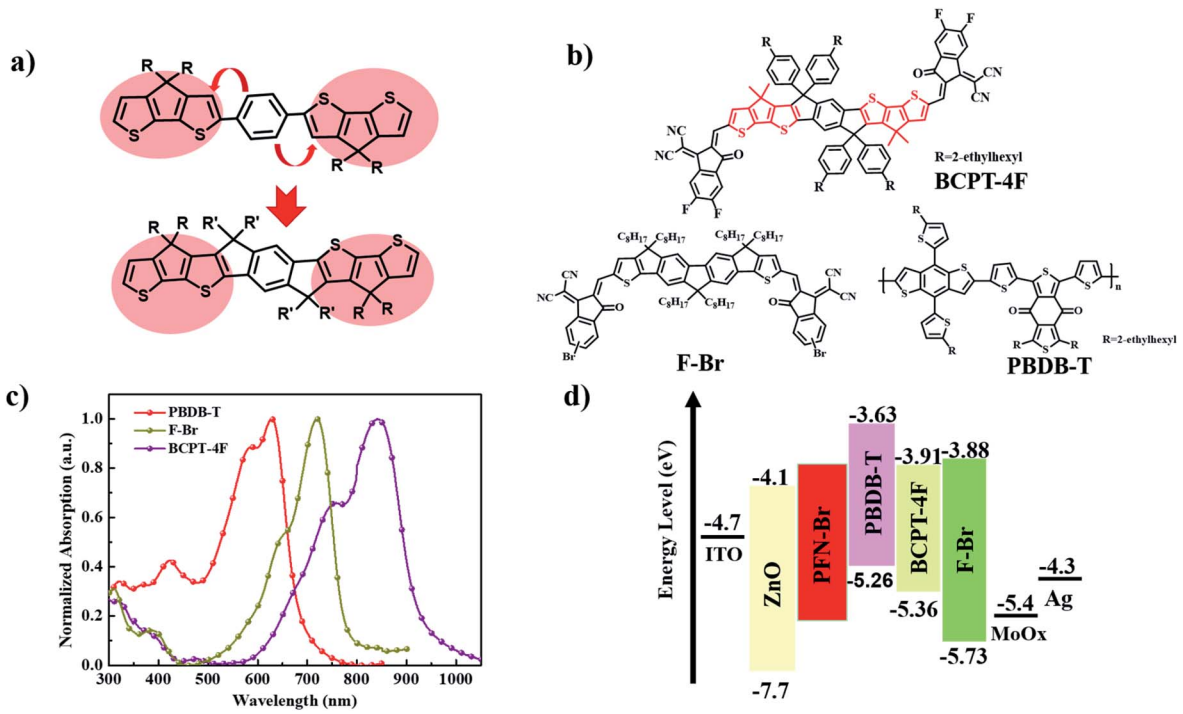

Fig. 1 (a) Design idea of the CPT fused acceptor; (b) chemical structure of PBDB-T, BCPT-4F, and F-Br; (c) normalized UV-vis absorption spectra of PBDB-T, F-Br, and BCPT-4F in neat films; (d) energy diagrams of all materials used in ternary solar cells.

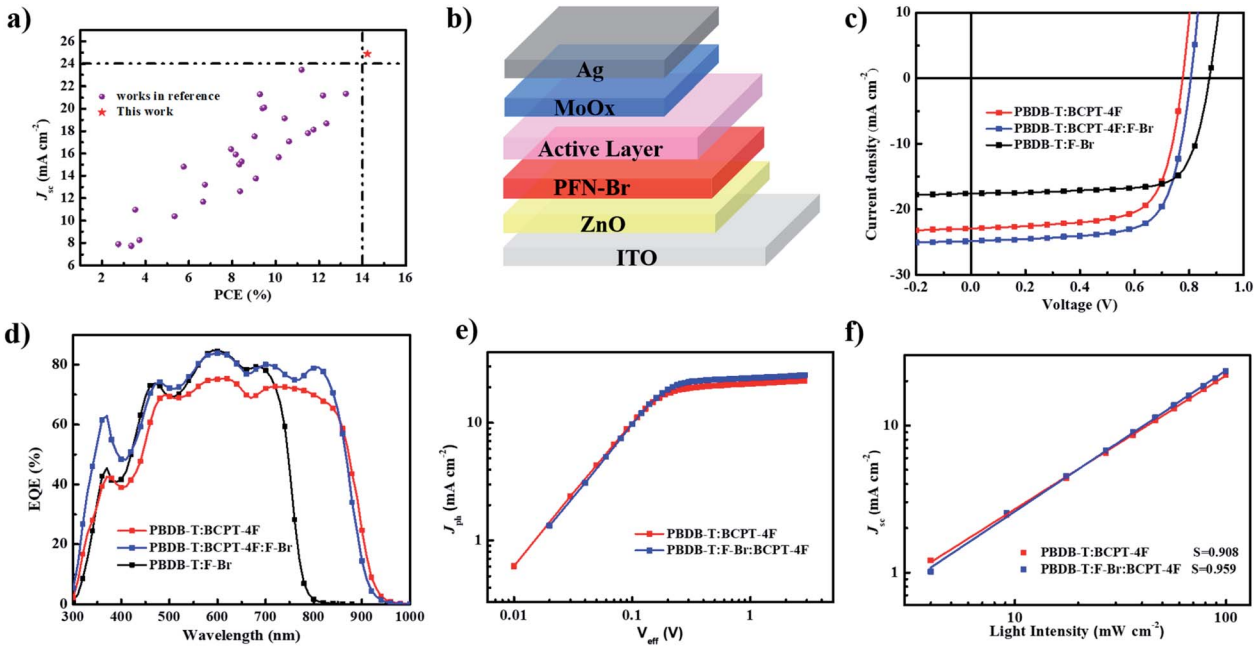

Fig. 2 (a) Comparison of the current PCEs of our work and of reported devices based on CPT-based molecules; (b) schematic diagram of the inverted device structure; (c) current density–voltage (J–V) curves of the binary and ternary devices under one sun illumination (AM 1.5 G 100 mW cm^{-2}); (d) EQE spectra of the corresponding devices; (e) J_{ph} *versus* V_{eff} and (f) light-intensity dependence of J_{sc} measurement of the devices.

fabricated to evaluate the photovoltaic performance using **BCPT-4F** as an acceptor. The wide-band gap polymer **PBDB-T** was selected as a donor due to its matched energy levels and complementary absorption with **BCPT-4F**.[28] Detailed device fabrication and optimization conditions, such as donor/acceptor weight ratio and thermal annealing temperature are provided in the ESI.† The current density–voltage (J–V) curves of the optimal devices are displayed in Fig. 2c, and their corresponding photovoltaic parameters are summarized in Table 2. When blended with **PBDB-T**, **BCPT-4F** based devices exhibit the best PCE of 12.43%, with a high J_{sc} of 22.96 mA cm^{-2}, a V_{oc} of 0.776 V and an FF of 0.698 (Fig. 2c). The high J_{sc} of the device compared to that of the unfused CPT based molecules is attributed to the redshifted UV-vis absorption.[36,37]

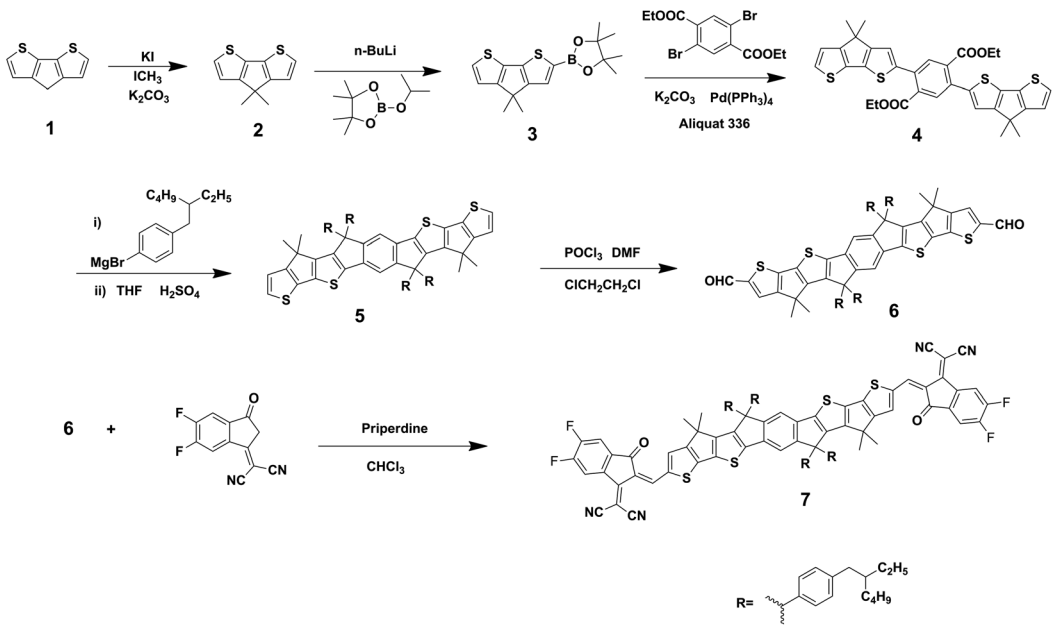

Scheme 1 Synthetic route for BCPT-4F.

Table 1 The optical and electrochemical properties of BCPT-4F

	λ_{max}^{CF} (nm)	λ_{max}^{film} (nm)	λ_{edge}^{film} (nm)	HOMO (eV)	LUMO (eV)	E_g^{CV} (eV)	E_g^{opt} (eV)
BCPT-4F	785	843	940	−5.36	−3.91	1.45	1.32

Table 2 Photovoltaic parameters of the optimized OPV binary and ternary devices

PBDB-T : BCPT-4F : F-Br	V_{oc} (V)	FF	J_{sc} (mA cm^{-2})	J_{sc}^{EQE} (mA cm^{-2})	PCE (%) (ave.)[a]
1 : 1 : 0	0.776	0.698	22.96	22.30	12.43 (12.18)
1 : 0.5 : 0.5	0.806	0.709	24.88	24.22	14.23 (14.08)
1 : 0 : 1	0.862	0.740	18.05	17.39	11.52 (11.36)

[a] All the PCEs are obtained with 4 significant digits and the average values are calculated from 10 devices.

A ternary device is a feasible and easy method to further improve the performance of the binary device.[5,38–40] Recently, our group reported a middle band gap molecule **F-Br** with an absorption spectrum located in the range of 550–750 nm.[35] As shown in Fig. 1c, **F-Br** shows complementary absorption with that of **PBDB-T** and BPCT-4F. Meanwhile, the **PBDB-T:F-Br** device delivered an efficiency over 11% with an outstanding FF of 0.74. In order to further improve the device performance, we fabricated ternary devices using **F-Br** as the third component. While systematically optimizing the ratio of **F-Br** and **BCPT-4F**, a best PCE of 14.23% is achieved with a J_{sc} of 24.88 mA cm^{-2}, a V_{oc} of 0.806 V and an FF of 0.709, when 50 wt% of **F-Br** was added (**PBDB-T : F-Br : BCPT-4F** = 1 : 0.5 : 0.5 in weight), which is presently the highest efficiency for devices with CPT based photovoltaic materials. Compared to the host binary device, the ternary device exhibited improved J_{sc}, V_{oc} and FF, simultaneously (Table 2). The external quantum efficiency (EQE) curves of the optimized binary and ternary devices are shown in Fig. 2d. The **PBDB-T:BCPT-4F** based binary device featured broad EQE values covering 300 to 940 nm. In contrast, **PBDB-T:BCPT-4F:F-Br** based ternary devices exhibited an enhanced EQE response with values over 70% in the region of 500–850 nm, suggesting that the ternary device featured a more efficient charge transfer between the donor and acceptor. The integral current density values calculated from the EQE curves of **PBDB-T:BCPT-4F** and **PBDB-T : BCPT-4F : F-Br** (1 : 0.5 : 0.5) were 22.30 mA cm^{-2} and 24.22 mA cm^{-2}, respectively, which are well in agreement with the J_{sc} from *J–V* measurements with deviations within 3%.

To probe the exciton/charge dynamics of the binary and ternary devices, we measured the photocurrent density (J_{ph}) *versus* the effective voltage (V_{eff}) to study charge generation, dissociation, and extraction properties (Fig. 2e). $J_{ph} = J_L - J_D$, where J_L is the current density under illumination and J_D is the current density in the dark. $V_{eff} = V_o - V_a$, where V_a is the applied voltage and V_o is the voltage at which J_{ph} is zero.[41,42] As depicted in Fig. 2e, J_{ph} increased with a rise in V_{eff} and when V_{eff} arrived at ~2 V, J_{ph} values for all the devices reached saturation (J_{sat}), indicating that the charge recombination of the devices is minimized at a higher voltage due to the high internal electric field in the devices. We also adopted the values of J_{ph}/J_{sat} to estimate the charge dissociation and charge collection probability ($P(E, T)$) in the devices. Under maximal power output conditions, the $P(E, T)$ were calculated to be 93% for the **BCPT-4F** based binary device and 94% for the ternary device. The improved value of the ternary device compared to the **BCPT-4F** based binary device indicated a better charge dissociation and collection of the ternary device.

To study the charge recombination in the devices, the light-intensity dependence (P) of J_{sc} was measured. According to the equation of $J_{sc} \propto P^{\alpha}$, the power-law exponent α implies the extent of bimolecular recombination. As shown in Fig. 2f, slopes of 0.908 and 0.959 were obtained for the **BCPT-4F** binary and ternary based devices, respectively. The ternary device showed the highest α values compared to the two binary devices, implying less bimolecular recombination in the ternary devices. It is consistent with the promoted EQE value and high J_{sc} of the ternary device. As shown in Fig. S16,† the V_{oc} is linearly dependent on the natural logarithm of light intensity with slopes of $1.27kT/q$ and $1.23kT/q$ for the binary and ternary devices, respectively, where k is the Boltzmann constant, T is the temperature in kelvin and q is the elementary charge. Generally, a deviation of the slope from kT/q reflects defect-assisted recombination in the devices.[43] The small slopes implied low trap density and weak trap-assistant recombination in the **BCPT-4F** based devices, especially in the ternary device. Furthermore, the space charge-limited current (SCLC) method was employed to study the charge transport properties of electron-only and hole-only devices.[44] As shown in Fig. S17,† the calculated electron and hole mobilities for the **PBDB-T:BCPT-4F** based devices are 2.85×10^{-4} and 4.54×10^{-4} cm^{-2} V^{-1} s^{-1}, respectively. After adding 50 wt% **F-Br**, the ternary blend film achieved a higher electron mobility of 3.63×10^{-4} cm^{-2} V^{-1} s^{-1} and a hole mobility of 3.76×10^{-4} cm^{-2} V^{-1} s^{-1} simultaneously. Despite the hole mobility decreasing, a balanced μ_h/μ_e was achieved, which is favourable for the overall charge collection and thus improved the FF, consistent with the device performance.

2.3 Morphology characterization

We employed grazing incidence wide-angle X-ray scattering (GIWAXS) to gain further insight into the molecular stacking and orientation of the binary and ternary blend films (Fig. 3a, b and S18†). As can be seen in Fig. S18,† **BCPT-4F** exhibits a clear π–π stacking diffraction peak (010) in the out-of-plane

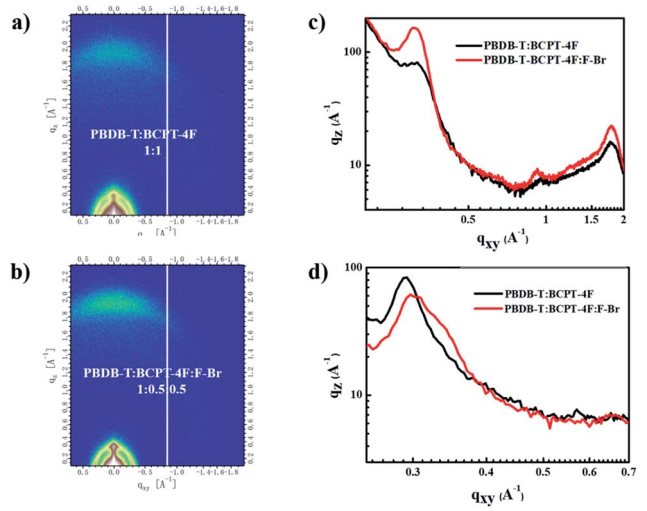

Fig. 3 (a) The GIWAXS patterns based on the BCPT-4F based binary blending film and (b) ternary blending film; (c) line-cut profiles of the OOP direction and (d) line-cut profiles of the IP direction.

(OOP) direction and a lamellar diffraction peak (100) in the in-plane (IP) direction, suggesting that the **BCPT-4F** neat film has a preferred face-on orientation relative to the substrate. Note that neat film of **PBDB-T** revealed a preferred face-on orientation, which is beneficial to charge transport. Out-of-plane (OOP) and in-plane (IP) line-cut profiles of GIWAXS for the binary and ternary blend films are presented in Fig. 3c and d. For binary blend films, the **PBDB-T:BCPT-4F** blend film exhibited two (010) diffraction peaks in the OOP (0.96 and 1.77 Å^{-1}) and one (100) in the IP (0.29 Å^{-1}) direction. All these diffraction peaks for the blend films implied face on orientation and good molecular packing. As for the ternary blend film (**PBDB-T : BCPT-4F : F-Br** = 1 : 0.5 : 0.5), the (100) diffraction peaks were located at 0.30 Å^{-1} in the IP direction and the (010) diffraction peaks were located at 0.93 and 1.79 Å^{-1} in the OOP direction. And the π–π stacking distances (d_π) were calculated to be 3.55 and 3.51 Å for the **BCPT-4F** based binary and ternary devices, respectively. From the Scherrer equation,[45] the crystal coherence length (CCL) in the (010) diffraction direction was estimated to be 20.49 Å for the **BCPT-4F** binary blend film, and 23.86 Å for the ternary device. The increased CCL and smaller d_π of the ternary blend film compared to the binary **BCPT-4F** blend film indicated that the introduction of a strong crystalline component, **F-Br** leads to more ordered molecular packing and a preferred morphology in the ternary device. The improved morphology with the addition of the third component **F-Br** has a positive effect on the charge dissociation and transport for the ternary device compared with the binary device, which is consistent with the increase of FF and J_{sc}, as discussed above.

3. Conclusions

In summary, a new acceptor **BCPT-4F** with a CPT fused backbone has been successfully designed and synthesized. Compared with non-fused analogous molecules, **BCPT-4F** possessed redshifted absorption with an onset around 1000 nm and a low band gap of 1.32 eV. The binary device based on **PBDB-T:BCPT-4F** achieved a PCE of 12.43%. A ternary device with **F-Br** as the third component was fabricated and achieved a PCE of 14.23% with a simultaneously improved V_{oc} of 0.806 eV, J_{sc} of 24.88 mA cm^{-2} and an FF of 0.709, and is presently the highest efficiency for devices with CPT based photovoltaic materials. These comprehensively improved parameters can be ascribed to the suppressed bimolecular recombination, improved charge dissociation and collection efficiency, balanced charge transport and the reduction of intermixing domain size. The results offer valuable insight into the new active layer-molecule design for higher performance OPVs.

Conflicts of interest

There are no conflicts of interest to declare.

Acknowledgements

The authors gratefully acknowledge the financial support from the MoST (2016YFA0200200 and 2019YFA0705900) and the NSFC (51773095, 21935007, and 51873089) of Tianjin city, China (17JCJQJC44500 and 17JCZDJC31100) and 111 Project (B12015).

Notes and references

1 H. Fu, Z. Wang and Y. Sun, *Angew. Chem., Int. Ed.*, 2019, **58**, 4442–4453.
2 A. J. Heeger, *Chem. Soc. Rev.*, 2010, **39**, 2354–2371.
3 J. Y. Kim, K. Lee, N. E. Coates, D. Moses, T.-Q. Nguyen, M. Dante and A. J. Heeger, *Science*, 2007, **317**, 222.
4 C. J. Traverse, R. Pandey, M. C. Barr and R. R. Lunt, *Nat. Energy*, 2017, **2**, 849–860.
5 Y. Wu, Y. Zheng, H. Yang, C. Sun, Y. Dong, C. Cui, H. Yan and Y. Li, *Sci. China: Chem.*, 2020, **63**, 265–271.
6 X. Xu, K. Feng, Z. Bi, W. Ma, G. Zhang and Q. Peng, *Adv. Mater.*, 2019, **31**, 1901872.
7 T. Yan, W. Song, J. Huang, R. Peng, L. Huang and Z. Ge, *Adv. Mater.*, 2019, **31**, 1902210.
8 Y. Cui, H. Yao, J. Zhang, T. Zhang, Y. Wang, L. Hong, K. Xian, B. Xu, S. Zhang, J. Peng, Z. Wei, F. Gao and J. Hou, *Nat. Commun.*, 2019, **10**, 2515.
9 B. Fan, D. Zhang, M. Li, W. Zhong, Z. Zeng, L. Ying, F. Huang and Y. Cao, *Sci. China: Chem.*, 2019, **62**, 746–752.
10 K. Li, Y. Wu, Y. Tang, M. A. Pan, W. Ma, H. Fu, C. Zhan and J. Yao, *Adv. Energy Mater.*, 2019, **9**, 1901728.
11 L. Meng, Y. Zhang, X. Wan, C. Li, X. Zhang, Y. Wang, X. Ke, Z. Xiao, L. Ding, R. Xia, H.-L. Yip, Y. Cao and Y. Chen, *Science*, 2018, **361**, 1094–1098.
12 M.-A. Pan, T.-K. Lau, Y. Tang, Y.-C. Wu, T. Liu, k. Li, M.-C. Chen, X. Lu, W. Ma and C. Zhan, *J. Mater. Chem. A*, 2019, **7**, 20713–20722.

13 L. Hong, H. Yao, Z. Wu, Y. Cui, T. Zhang, Y. Xu, R. Yu, Q. Liang, B. Gao, K. Xian, H. Y. Woo, Z. Ge and J. Hou, *Adv. Mater.*, 2019, **31**, 1903441.
14 Z. Luo, R. Sun, C. Zhong, T. Liu, G. Zhang, Y. Zou, X. Jiao, J. Min and C. Yang, *Sci. China: Chem.*, 2020, DOI: 10.1007/s11426-019-9670-2.
15 R. Ma, T. Liu, Z. Luo, Q. Guo, Y. Xiao, Y. Chen, X. Li, S. Luo, X. Lu, M. Zhang, Y. Li and Y. He, *Sci. China: Chem.*, 2020, DOI: 10.1007/s11426-019-9669-3.
16 A. Wadsworth, M. Moser, A. Marks, M. S. Little, N. Gasparini, C. J. Brabec, D. Baran and I. McCulloch, *Chem. Soc. Rev.*, 2019, **48**, 1596–1625.
17 J.-S. Wu, S.-W. Cheng, Y.-J. Cheng and C.-S. Hsu, *Chem. Soc. Rev.*, 2015, **44**, 1113–1154.
18 G. Zhang, J. Zhao, P. C. Y. Chow, K. Jiang, J. Zhang, Z. Zhu, J. Zhang, F. Huang and H. Yan, *Chem. Rev.*, 2018, **118**, 3447–3507.
19 Y. Chen, X. Wan and G. Long, *Acc. Chem. Res.*, 2013, **46**, 2645–2655.
20 B. Kan, H. Feng, X. Wan, F. Liu, X. Ke, Y. Wang, Y. Wang, H. Zhang, C. Li, J. Hou and Y. Chen, *J. Am. Chem. Soc.*, 2017, **139**, 4929–4934.
21 J. Hou, O. Inganäs, R. H. Friend and F. Gao, *Nat. Mater.*, 2018, **17**, 119–128.
22 J. Yuan, Y. Zhang, L. Zhou, G. Zhang, H.-L. Yip, T.-K. Lau, X. Lu, C. Zhu, H. Peng, P. A. Johnson, M. Leclerc, Y. Cao, J. Ulanski, Y. Li and Y. Zou, *Joule*, 2019, **3**, 1140–1151.
23 S. Li, L. Zhan, F. Liu, J. Ren, M. Shi, C.-Z. Li, T. P. Russell and H. Chen, *Adv. Mater.*, 2018, **30**, 1705208.
24 Y. Cui, G. Jia, J. Zhu, Q. Kang, H. Yao, L. Lu, B. Xu and J. Hou, *Chem. Mater.*, 2018, **30**, 1078–1084.
25 C. V. Kumar, L. Cabau, E. N. Koukaras, A. Viterisi, G. D. Sharma and E. Palomares, *J. Mater. Chem. A*, 2015, **3**, 4892–4902.
26 C. K. Lo, B. R. Gautam, P. Selter, Z. Zheng, S. D. Oosterhout, I. Constantinou, R. Knitsch, R. M. W. Wolfe, X. Yi, J.-L. Brédas, F. So, M. F. Toney, V. Coropceanu, M. R. Hansen, K. Gundogdu and J. R. Reynolds, *Chem. Mater.*, 2018, **30**, 2995–3009.
27 P. Cheng, G. Li, X. Zhan and Y. Yang, *Nat. Photonics*, 2018, **12**, 131–142.
28 Y.-Q.-Q. Yi, H. Feng, N. Zheng, X. Ke, B. Kan, M. Chang, Z. Xie, X. Wan, C. Li and Y. Chen, *Chem. Mater.*, 2019, **31**, 904–911.
29 S. Li, L. Zhan, F. Liu, J. Ren, M. Shi, C.-Z. Li, T. P. Russell and H. Chen, *Adv. Mater.*, 2018, **30**, 1705208.
30 H. Huang, Q. Guo, S. Feng, C. e. Zhang, Z. Bi, W. Xue, J. Yang, J. Song, C. Li, X. Xu, Z. Tang, W. Ma and Z. Bo, *Nat. Commun.*, 2019, **10**, 3038.
31 Y.-Q.-Q. Yi, H. Feng, X. Ke, J. Yan, M. Chang, X. Wan, C. Li and Y. Chen, *J. Mater. Chem. C*, 2019, **7**, 4013–4019.
32 J. Sun, X. Ma, Z. Zhang, J. Yu, J. Zhou, X. Yin, L. Yang, R. Geng, R. Zhu, F. Zhang and W. Tang, *Adv. Mater.*, 2018, **30**, 1707150.
33 S. Li, L. Zhan, W. Zhao, S. Zhang, B. Ali, Z. Fu, T.-K. Lau, X. Lu, M. Shi, C.-Z. Li, J. Hou and H. Chen, *J. Mater. Chem. A*, 2018, **6**, 12132–12141.
34 R. Zheng, Q. Guo, D. Hao, C. e. Zhang, W. Xue, H. Huang, C. Li, W. Ma and Z. Bo, *J. Mater. Chem. C*, 2019, **7**, 15141–15147.
35 Y. Wang, Y. Zhang, N. Qiu, H. Feng, H. Gao, B. Kan, Y. Ma, C. Li, X. Wan and Y. Chen, *Adv. Energy Mater.*, 2018, **8**, 1702870.
36 S. Li, L. Zhan, C. Sun, H. Zhu, G. Zhou, W. Yang, M. Shi, C.-Z. Li, J. Hou, Y. Li and H. Chen, *J. Am. Chem. Soc.*, 2019, **141**, 3073–3082.
37 L. Zhan, S. Li, S. Zhang, T.-K. Lau, T. R. Andersen, X. Lu, M. Shi, C.-Z. Li, G. Li and H. Chen, *Sol. RRL*, 2019, **3**, 1900317.
38 R. Geng, X. Song, H. Feng, J. Yu, M. Zhang, N. Gasparini, Z. Zhang, F. Liu, D. Baran and W. Tang, *ACS Energy Lett.*, 2019, **4**, 763–770.
39 B. Kan, Y.-Q.-Q. Yi, X. Wan, H. Feng, X. Ke, Y. Wang, C. Li and Y. Chen, *Adv. Energy Mater.*, 2018, **8**, 1800424.
40 T. Liu, Z. Luo, Q. Fan, G. Zhang, L. Zhang, W. Gao, X. Guo, W. Ma, M. Zhang, C. Yang, Y. Li and H. Yan, *Energy Environ. Sci.*, 2018, **11**, 3275–3282.
41 C. M. Proctor, M. Kuik and T.-Q. Nguyen, *Prog. Polym. Sci.*, 2013, **38**, 1941–1960.
42 P. W. M. Blom, V. D. Mihailetchi, L. J. A. Koster and D. E. Markov, *Adv. Mater.*, 2007, **19**, 1551–1566.
43 S. R. Cowan, A. Roy and A. J. Heeger, *Phys. Rev. B: Condens. Matter Mater. Phys.*, 2010, **82**, 245207.
44 Y. Zhang, H. Feng, L. Meng, Y. Wang, M. Chang, S. Li, Z. Guo, C. Li, N. Zheng, Z. Xie, X. Wan and Y. Chen, *Adv. Energy Mater.*, 2019, **9**, 1902688.
45 D.-M. Smilgies, *J. Appl. Crystallogr.*, 2009, **42**, 1030–1034.